MIXED CONVECTION ANALYSIS IN A DUAL-DRIVEN CAVITY WITH A STABLE VERTICAL TEMPERATURE GRADIENT USING THE LATTICE BOLTZMANN METHOD

by

Muhammad HARIS[a*], Shams ul ISLAM[a], and Zia ul ISLAM[b]

[a]Department of Mathematics, COMSATS University Islamabad,
Park Road Chak Shahzad, Islamabad, Pakistan
[b]Shenzhen Graduate School, Harbin Institute of Technology,
Shenzhen University Town, Shenzhen, China

Original scientific paper
https://doi.org/10.2298/TSCI240627241H

The complex dynamics of mixed convection circumstances, concentrating on two examples. In the first case, mixed convection was investigated in a single-sided lid-driven cavity with a top and bottom walls arrangement and the second scenario explores parallel and anti-parallel topologies, focusing on mixed convection in a double-sided lid-driven cavity. The main parameters in this study are the Reynolds, Rayleigh, Prandtl, Grashof, and Richardson numbers. Calculation of numerical solutions to the Navier-Stokes equations over wide ranges in parameters, $0 \le Gr \le 10^6$, $0 \le Re \le 3000$, $Pr \sim O(1)$, *and an aspect ratio approximately* $O(1)$. *The study analyzes these results systematically to understand the relative importance of natural convection and forced convection. As a result of this study, a 2-D cavity with specific boundary conditions was created. In a square domain with adiabatic side walls, a top wall is maintained at a higher temperature than the bottom wall. The flow characteristics approach those of a typical driven-cavity of a non-stratified fluid when* $Gr/Re^2 \le 1$. *There are low fluctuations in temperature and well-mixed fluids throughout the majority of the interior. Much of the inner cavity's middle and bottom are stationary when* $Gr/Re^2 \gg 1$. *Temperature patterns in these areas are vertically linear and isotherms are nearly horizontal. Lattice Boltzmann method considers the effect of gravity on mixed convection by adjusting the* y*-velocity using a temperature-dependent forcing factor. The calculation of the Nusselt number at the top wall reveals enhanced heat transfer, with the results suggesting increased intensity when* $Gr/Re^2 \ll 1$.

Key words: *mixed convection, heat transfer enhancement, square cavity, lid-driven, lattice Boltzmann method*

Introduction

In a variety of technical and industrial situations, as well as in natural settings, mixed convection flows are common. Examples include heat exchangers operating at low speeds, fan-cooled electronics, nuclear reactor emergency cooling, solar receivers exposed to wind current, and fluid dynamics in atmospheric and oceanic systems [1-3]. Natural convection and forced

*Corresponding author, e-mail: muhammadharis9138@gmail.com

convection are the two main forms of fluid movement that combine to produce mixed convection. Because warmer fluid rises and colder fluid sinks because of its higher density, natural convection occurs when the buoyancy force is the source of fluid movement. This creates a continuous cycle. Conversely, forced convection actively moves fluid and heat and is driven by an outside source, such as a pump, fan, or rotating plate. The ratio of the Grashof number to the square of the Reynolds number known as the Richardson number, controls the balance between the forced and natural convection mechanisms in mixed convection situations. Systems used to explore the phenomenon include heated lid-driven cavities. In this system, buoyancy-driven natural convection is introduced by gravity, and moving plates induce forced convection.

The rectangular or cubic container is one of the basic geometric arrangements for studying fluid dynamics. Under such circumstances, the tangential motion of the bounding wall inside the plane becomes an important mechanical driver for uniformly-density liquids and provides a simple domain. A cuboid wall that moves perpendicular to itself characterizes a lid-driven cavity. Its simplicity has drawn a lot of interest to the lid-driven cavity, which may be utilized as a laboratory and benchmark issue for numerical research into certain physical processes. The Reynolds number, defined as $\mathrm{Re} = U_0 h/\nu$ and the cavity aspect ratio, A, defined as $A = h/b$, are the two main non-dimensional variables that describe this flow. The parameters h and b denote the height and width of the cavity in these formulations, the fluid's kinematic viscosity, ν, and the velocity of the top boundary wall, U_0. Attempts to correlate these computational outcomes with experimental data have been made in addition to the many computer studies that have been carried out and documented in the literature [4-9].

Introduced into the cavity side walls, a temperature gradient offers a significant dynamic component. Temperature and velocity within the cavity are influenced by the buoyancy effect created by the temperature difference. A further understanding of basic fluid dynamics and practical engineering issues can be obtained by studying this mixed-driven natural convection flow with internal constraints. The investigative results on mixed convective flow in a hollow square cavity have been published by Iwastu *et al.* [10]. With their research, they built upon the findings of Mohamad and Viskanta [11]. Research on mixed convective flow in a shallow cavity with $A \ll 1$ was reported by Mohammad and Viskanta [11]. It is important to note that in their investigation, the top sliding wall temperature was lower than the fixed bottom wall. The two vertical side walls were covered with thermal insulation. The flow consequently becomes gravitationally unstable.

A study conducted by Iwatsu *et al.* [10] investigated the thermal energy transfer control in a system with a sliding top wall. The top wall temperature was constantly set higher than the bottom wall. This system was working fine with primary conduction use for heat conduct. The authors decided that conduction was leading in the mechanism of the heat transfer process with very slight forced convection. Moreover, the statement about maintaining the uniform vertical temperature gradient throughout the system was confirmed. The primary task was to develop the velocity profiles and explain why the heat transfer rate was increasing while the upper wall was moving in its plane at a constant rate of velocity due to the external driving force. The Reynolds number and Rayleigh number were varied throughout the investigations to capture a broad collection of flow features.

The lattice Boltzmann method (LBM) has been used to study mixed convection in a driven cavity with different fluid types and boundary conditions throughout the past 20 years [12-16]. A Cu-water nanofluid was employed by Karimipour *et al.* [12] to investigate mixed convection in an inclined cavity. After looking into mixed convection, they found that natural

convection, forced convection, and mixed convection dominated at different Richardson numbers, Ri = 0.1, Ri = 1, and Ri = 10. Mixed convection was studied by Guo *et al.* [13] for various A and Richardson number. They found that the relative importance of forced and natural convection modes in heat transfer could be ascertained using the Richardson number. Using various relaxation periods LBM, Bettaibi *et al.* [14] investigated mixed convection in a cavity heated differently and found that heat transported increased in terms of Nusselt number as Richardson number decreased. By passing a nanofluid through a square chamber with a wavy bottom wall, Abu-Nada and Chamkha [15] studied mixed convection. They found that for all values of the Richardson number, the introduction of nanoparticles significantly improved heat transfer. Oztop *et al.* [16] investigated mixed convection in a driven cavity in the presence of a magnetic field with a heated bottom corner using a broad range of Hartmann number. They found that heat transfer is decreased when the Hartmann number is raised. Therefore, the magnetic field plays a crucial role in regulating the flow of fluids and the transfer of heat.

The fluid-flow and related heat transfer are mainly characterized by four dimensionless parameters, *i.e.*: Re, Gr, A, and Pr, as recognized in the non-dimensionalized governing equations. During the subsequent discussions, the Prandtl number is often set at Pr = 0.71 (the case of air) and the aspect ratio is fixed at $A = 1.0$ (a square cavity). This will enable an assessment of the specific effects of natural convection (represented by Grashof number) and forced convection (represented by Reynolds number). The ratio Gr/Re^2 emerges as a measure of the relative importance of natural convection to forced convection.

As mixed convection is used in so many significant industrial applications such as the cooling of electrical components, float glass manufacturing, nuclear reactors, electronic equipment, and microelectronic devices it is one of the most discussed issues in thermodynamics. It is a fundamental process in heat transfer that is widely used in various industries for flow and heat transfer within a lid-driven cavity. This study looks at the basic dynamics of mixed convection in a cavity driven by a lid, concentrating on four different scenarios: These are top lid-driven, bottom lid-driven, moving parallel, and moving anti-parallel. Through these possibilities, it is intended to provide clarification concerning the discussed issue, the effects of forced convection on the fluid-flow and a global heat transfer. To this adding the moving lid creates forced convection flow over the cavity, when it combines with buoyancy-induced natural convection leads to a complicated temperature and velocity distribution within the cavity. This work reveals the complex relationship between the flow, convection process, and the motion of the lid in these four configurations.

Problem and solution methodology

Problem specification

The schematic flow of the problem is represented in figs. 1(a)-1(d). Heat transport and fluid-flow are modeled using LBM in the 2-D cavity with a length equal to the chosen grid size. The cavity's vertical walls are considered to be adiabatic, with the lower lid being maintained at a lower temperature, $T_0 = 0$, and the upper lid being maintained at a higher temperature, $T_h = 1$. In the first validation scenario, the lower lid stays fixed while the top lid moves at a velocity of U_0 to the right. In the second situation, the lower lid travels to the right with the same velocity U_0 while the top lid remains stationary. In the third scenario, the top and bottom lids move in the same direction to the right with a velocity of U_0. In the fourth situation, the upper and lower lids share the velocity U_0 as they travel in the opposite direction. The Boussinesq approximation accounts for the density fluctuation in these simulations, which assumes laminar flow.

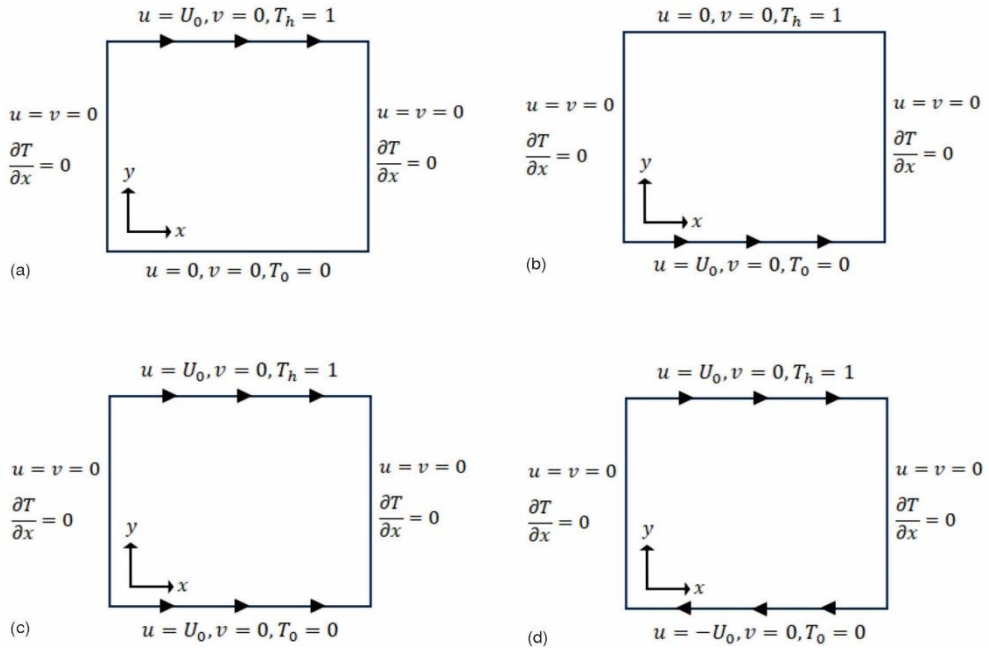

Figure 1. The boundary parameters for four mixed convection situations; (a) top lid-driven, (b) bottom lid-driven, (c) moving parallel, and (d) moving anti-parallel

Dimensionless mixed convection equations

An essential component of CFD is the Navier-Stokes equations. Several numerical techniques including finite volume, finite difference, and finite element approaches, are utilized to determine important fluid parameters like temperature, velocity, and pressure. These methods convert differential equations governed by specific boundaries and initial conditions into a set of algebraic equations. The governing equations for our issue, for incompressible fluid-flow, are given in the dimensional form as the continuity equation:

$$\nabla \boldsymbol{V} = 0 \tag{1}$$

momentum equation:

$$\frac{\partial \boldsymbol{V}}{\partial t} + (\boldsymbol{V}\nabla)\boldsymbol{V} = -\nabla \hat{p} + \frac{1}{\mathrm{Re}}\nabla^2 \boldsymbol{V} + \frac{\mathrm{Gr}}{\mathrm{Re}^2} T\boldsymbol{e} \tag{2}$$

and energy equation:

$$\frac{\partial T}{\partial t} + (\boldsymbol{V}\nabla)T = \frac{1}{\mathrm{PrRe}}\nabla^2 T \tag{3}$$

Non-isothermal flows are handled with this technique, eliminating the need to solve the compressible Navier-Stokes equations. It is assumed that density changes only significantly impact buoyancy forces and have a small effect on the flow field. The symbols ρ, $\hat{p}$, T, and ν, respectively, stand for the fluid's density, pressure, temperature, and kinematic viscosity, ∇ represents the nabla operator, and $\boldsymbol{V} = (u,v)$ represents the macroscopic velocities. The unit vector $\boldsymbol{e} = (0,1)$ indicates the buoyancy force's direction.

In this study, the Richardson number is used to evaluate the contribution of the natural and forced convection during the mixed convection process by comparing the ratio of the Grashof number and the square of the Reynolds number. According to the results, if $\mathrm{Gr}/\mathrm{Re}^2 \gg 1$ affects natural convection, the temperature distributions are almost vertical and isotherms are nearly horizontal, which results in considerable changes in temperature and fluid-flow. On the other hand, if $\mathrm{Gr}/\mathrm{Re}^2 \leq 1$, forced convection dominates meaning that the fluids within the cavity are well mixed and temperatures vary little across the cavity.

Lattice Boltzmann methodology

In CFD, the LBM is a popular and efficient technique that provides an indirect solution to the Navier-Stokes equations. Some of the various disciplines in which LBM finds applications are modeling incompressible flows, image processing, biomedical flows, blood vessel flows, multiphase flows, porous media flows, chemical reactions, and more. Its benefits over conventional computing approaches are evident.

The attributes of a group of fluid particles are described by distribution functions, which are used in LBM to model the behavior of a fluid. In the context of incompressible thermal flow issues, the double population thermal LBM describes the flow and temperature fields using two distinct distribution functions, F and G [17, 18]. To aid in its numerical solution, the governing equation of the LBM-BGK [19] is discretized using the Bhatnagar-Gross-Krook (BGK) approximation [20] can be written.

To compute fluid-flow:

$$F_i\left(x+\boldsymbol{e}_i\Delta t, t+\Delta t\right)-F_i\left(x,t\right)=-\frac{\Delta t}{\tau_v}\left[F_i\left(x,t\right)-F_i^{\mathrm{eq}}\left(x,t\right)\right]+f \tag{4}$$

To compute temperature:

$$G_i\left(x+\boldsymbol{e}_i\Delta t, t+\Delta t\right)-G_i\left(x,t\right)=-\frac{\Delta t}{\tau_T}\left[G_i\left(x,t\right)-G_i^{\mathrm{eq}}\left(x,t\right)\right] \tag{5}$$

where $\boldsymbol{e}_i$ is the discrete particle vector velocity in the i^{th} direction, x symbolizes a particle location at time t, the equilibrium distribution function for the flow and temperature fields is represented by $F_i^{\mathrm{eq}}(x,t)$ and $G_i^{\mathrm{eq}}(x,t)$, respectively, and the time step Δt is taken to be equal to one. The relaxation times for flow and temperature are represented by τ_v and τ_T, respectively, and in this study, they fall between 0.5 and 0.8. It also takes into consideration the buoyancy force component, f, using the Boussinesq approximation.

The velocities are discretized differently than the space and time discretization, which are done as normal. Velocity is applied to particles in a predetermined number of directions. The particles in the current investigation are given velocities as shown in fig. 2 of the D2Q9 model. The definition of the discrete particle velocities is:

$$\boldsymbol{e}_i=\begin{cases}\left(0,0\right) & \text{if } i=0\\ \left(\cos\left(\dfrac{\pi\left(i-1\right)}{4}\right),\ \sin\left(\dfrac{\pi\left(i-1\right)}{4}\right)\right) & \text{if } i=1,2,3,4\\ \left(\sqrt{2}\cos\left(\dfrac{\pi\left(i-1\right)}{4}\right),\ \sqrt{2}\sin\left(\dfrac{\pi\left(i-1\right)}{4}\right)\right) & \text{if } i=5,6,7,8\end{cases} \tag{6}$$

In eqs. (4) and (5), respectively, the local equilibrium distribution function terms $F_i^{\mathrm{eq}}(x,t)$ and $G_i^{\mathrm{eq}}(x,t)$ are used. They may be expressed as:

$$F_i^{\mathrm{eq}}\left(x,t\right)=\rho\omega_i\left[1+\frac{3\left(\boldsymbol{e}_i\boldsymbol{u}\right)}{c_s^2}+\frac{9\left(\boldsymbol{e}_i\boldsymbol{u}\right)^2}{2c_s^4}-\frac{3\left(\boldsymbol{u}\boldsymbol{u}\right)}{2c_s^2}\right] \tag{7}$$

$$G_i^{\mathrm{eq}}\left(x,t\right)=T\omega_i\left[1+\frac{3\left(\boldsymbol{e}_i\boldsymbol{u}\right)}{c_s^2}\right] \tag{8}$$

where ρ is the fluid density, $\boldsymbol{u}$ – the macroscopic velocity vector, and c_s – the speed of sound. The lattice weights ω_i are given by:

$$\omega_i=\begin{cases}4/9 & \text{if } i=0\\ 1/9 & \text{if } i=1,2,3,4\\ 1/36 & \text{if } i=5,6,7,8\end{cases} \tag{9}$$

The relaxation time is related to the thermal diffusivity, α, and kinematic viscosity, ν, in the following ways [21]:

$$\alpha=0.5c_s^2\left(\tau_T-0.5\right) \text{ and } \nu=0.5c_s^2\left(\tau_v-0.5\right) \tag{10}$$

Table 1 displays the weighting factors and discrete particle velocity vector for the D2Q9 lattice design. The D2Q9 model's lattice arrangement is shown in fig. 2.

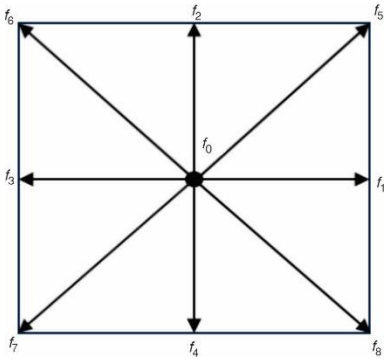

Figure 2. The sketch of D2Q9 model

Table 1. Weight distributions and vectors of velocity for lattice configurations in D2Q9

i	ω_i	$\boldsymbol{e}_i$
0	4/9	(0,0)
1	1/9	(1,0)
2		(0,1)
3		(–1,0)
4		(0,–1)
5	1/36	(1,1)
6		(–1,1)
7		(–1,–1)
8		(1,–1)

The distribution function makes it simple to list macroscopic quantities like density, velocity, and temperature as:

$$\rho=\sum_{i=0}^{8}F_i,\ \boldsymbol{u}=\frac{1}{\rho}\sum_{i=0}^{8}\boldsymbol{e}_iF_i, \text{ and } T=\sum_{i=0}^{8}G_i \tag{11}$$

Code validation

To verify the validity of our custom code, we first look at the streamline patterns and temperature isotherms at Re = 10^3 and Gr = 10^6. The results presented by Iwatsu *et al.* [10] show a high agreement with our findings, which are illustrated in the figure and tables. As shown in fig. 3, which presents a side-by-side comparison for and Re = 10^3 and Gr = 10^6, we

give a thorough analysis of the streamline patterns and temperature isotherms in the next section.

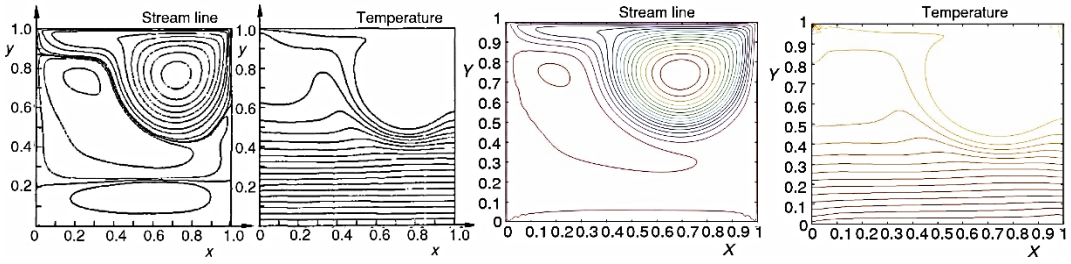

Figure 3. A comparison of the streamlines and isotherms between; (a) [10] and (b) the current findings at Re = 10^3 and Gr = 10^6

Comparisons of the maximum and minimum values of the horizontal and vertical velocities at the mid-section of the cavity between the present solution using LBM and the works by Iwatsu *et al.* [10] using FDM for a given Reynolds and Grashof numbers are tabs. 2 and 3.

Table 2. Comparison of the current results with those from Iwatsu *et al.* [10] at Re = 10^2 and Gr = 10^2

Re = 10^2	u_{min}	u_{max}	v_{min}	v_{max}
Iwatsu *et al*. [10]	–0.2037	1.0000	–0.2448	0.1699
Present results	–0.2122	1.0000	–0.2404	0.1718

Table 3. Comparison of the current results with those from Iwatsu *et al.* [10] at Re = 10^3 and Gr = 10^2

Re = 10^3	u_{min}	u_{max}	v_{min}	v_{max}
Iwatsu *et al*. [10]	–0.3781	1.0000	–0.5178	0.3658
Present results	–0.4006	1.0000	–0.5254	0.3821

Results and discussions

Grid independence analysis was performed for grid sizes between 101 × 101 and 141 × 141. The results showed that a 101 × 101 grid is enough to get accurate results. A comparative analysis for Re = 10^2, Gr = 10^2, and Pr = 0.71 showed that the 101 × 101 grid had a discrepancy of <2% with the 121 × 121 grid and <1% with the 141 × 141 grid in velocity and temperature. Therefore, the 101 × 101 grid was chosen for further simulations to balance accuracy and computational efficiency. One important parameter for differentiating between forced convection caused by the movement of the lid and buoyancy-driven natural convection is the Richardson number which is represented as the ratio Gr/Re^2. Although our analysis emphasizes the importance of buoyancy effects, it closely follows the conclusions of Iwatsu *et al.* [10] especially when considering a simple cavity. We observe several circumstances when $Ri \ll 1$. First, as seen by the horizontal and vertical velocity profiles along $x = 0.5$ and $y = 0.5$ in figs. 4(a)-4(d), mechanical forces excess buoyancy effects as the top lid moves. Second, a new dynamic occurs in the event of the bottom lid sliding, demonstrating the complex interaction between buoyancy and mechanical forces. Furthermore, different velocity profiles arise when both lids move in parallel or anti-parallel, providing insight into the complex relationships within the system. These thorough results offer a better comprehension of the intricate convection dynamics under various lid movement situations and how they affect Richardson number.

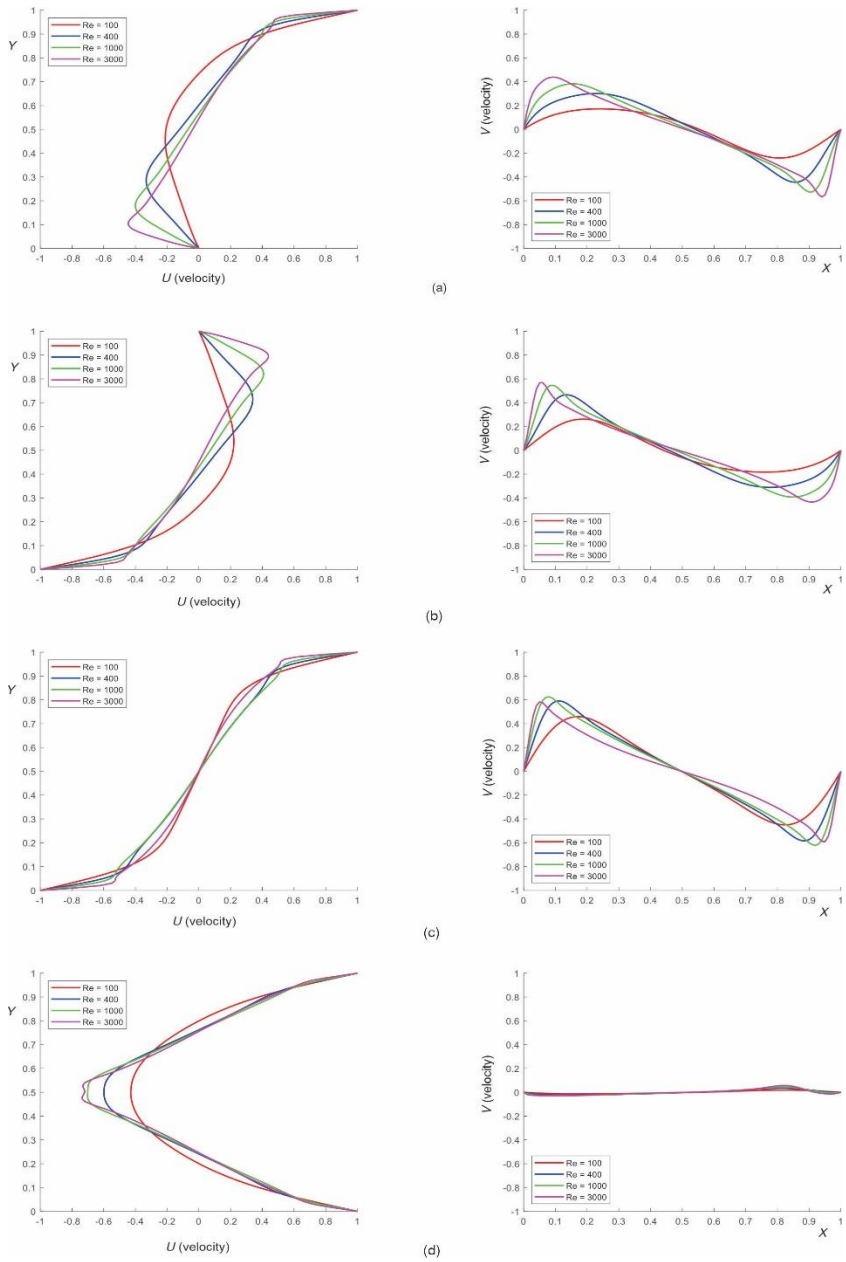

Figure 4. Profiles of horizontal and vertical velocity at Gr = 10^2 and Pr = 0.71; (a) top lid-driven, (b) bottom lid-driven, (c) moving parallel, and (d) moving anti-parallel

Moreover, where $\mathrm{Ri} \gg 1$, buoyancy's effect takes dominance over the sliding lid's mechanical effect. Figures 5(a)-5(d) shows a velocity profile that compares the instances of $Ri \gg O(1)$ and $\mathrm{Ri} \ll 1$. In particular, $\mathrm{Ri} \gg O(1)$ for Re = 100, 400, 1000, and 3000 at Gr = 10^6 demonstrating that buoyancy effects are significant. As a result, in these circumstances, the fluid is rather static over the bulk of the cavity.

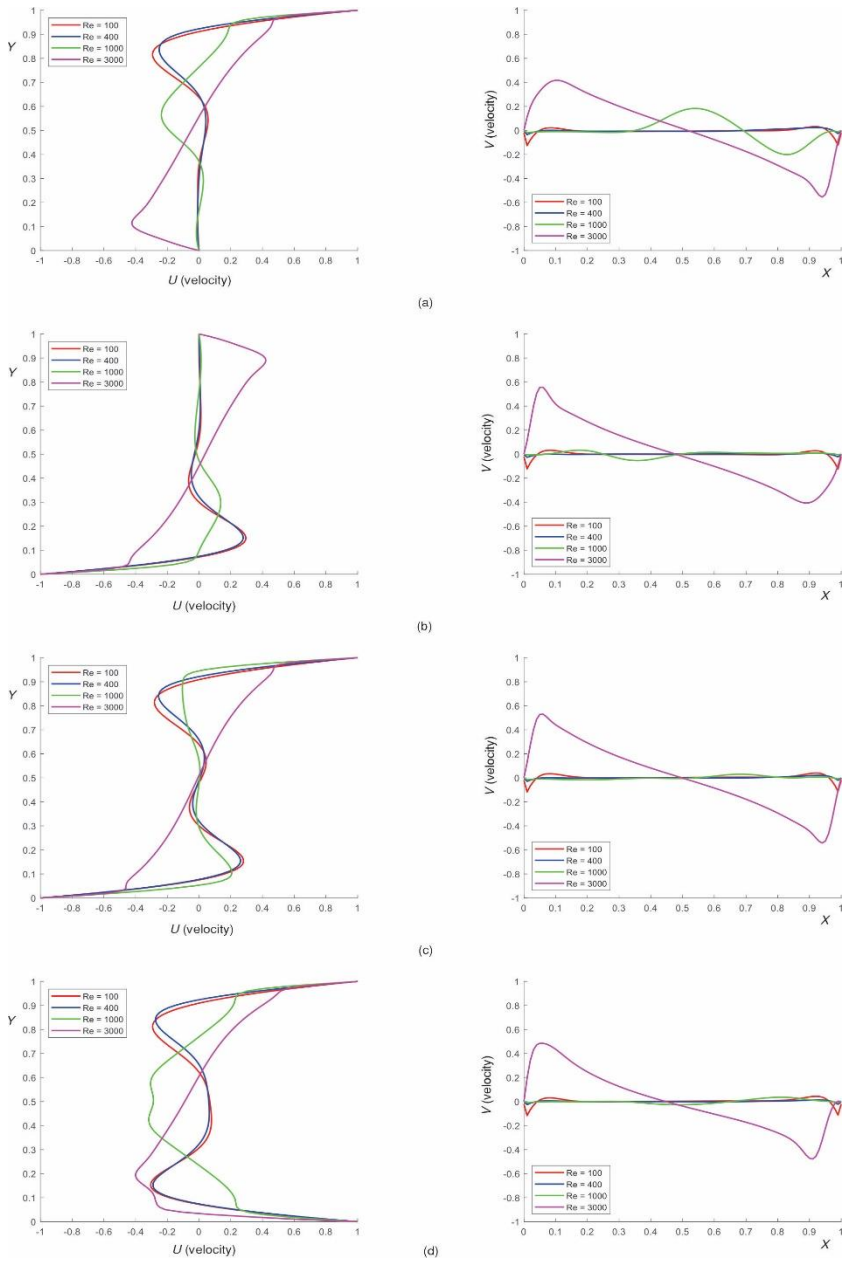

Figure 5. Profiles of horizontal and vertical velocity at Gr = 10^6 and Pr = 0.71; (a) top lid-driven, (b) bottom lid-driven, (c) moving parallel, and (d) moving anti-parallel

Modifying the numerical results in figs. 6(a)-6(d) shows how the basic flow characteristics evolve with increasing Grashof numberat constant Reynolds number. These findings demonstrate the expected change in the main flow pattern as previously mentioned, with $\mathrm{Ri} \gg O(1)$ and $\mathrm{Ri} \ll 1$ requirements constantly met. The condition $\mathrm{Gr}/\mathrm{Re}^2 \leq O(1)$ is securely satisfied at (Gr = 10^2 and 10^4) or not (Gr = 10^6) indicating the shift in the primary flow pattern.

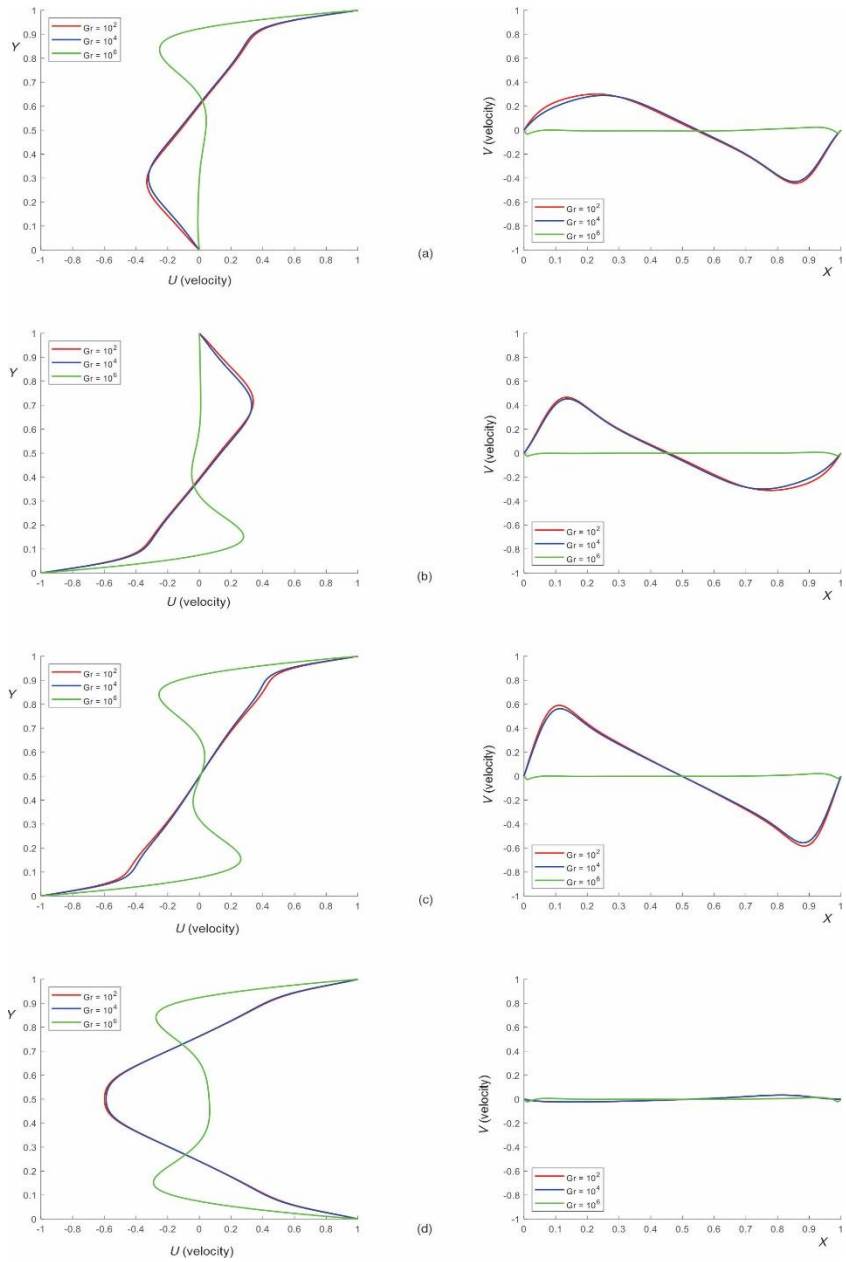

Figure 6. Profiles of horizontal and vertical velocity at Re = 400 and Pr = 0.71; (a) top lid-driven, (b) bottom lid-driven, (c) moving parallel, and (d) moving anti-parallel

The fluid-flow and temperature fields are visually depicted in figs. 7(a)-7(d) and 8(a)-8(d), providing valuable insights into the dynamics of the cavity under various driving conditions. Figures 7(a)-7(d) depicts a scenario in which buoyancy effects are relatively insignificant $\mathrm{Gr}/\mathrm{Re}^2 \ll 1$, similar to conventional mechanically-driven cavity flows. The observed gross flow characteristics in this particular case bear a strong resemblance to the fluid-

flow patterns exhibited by non-stratified fluid-flows with similar Reynolds number The primary circulation extends throughout the entire cavity, accompanied by smaller cells located near the lower corners.

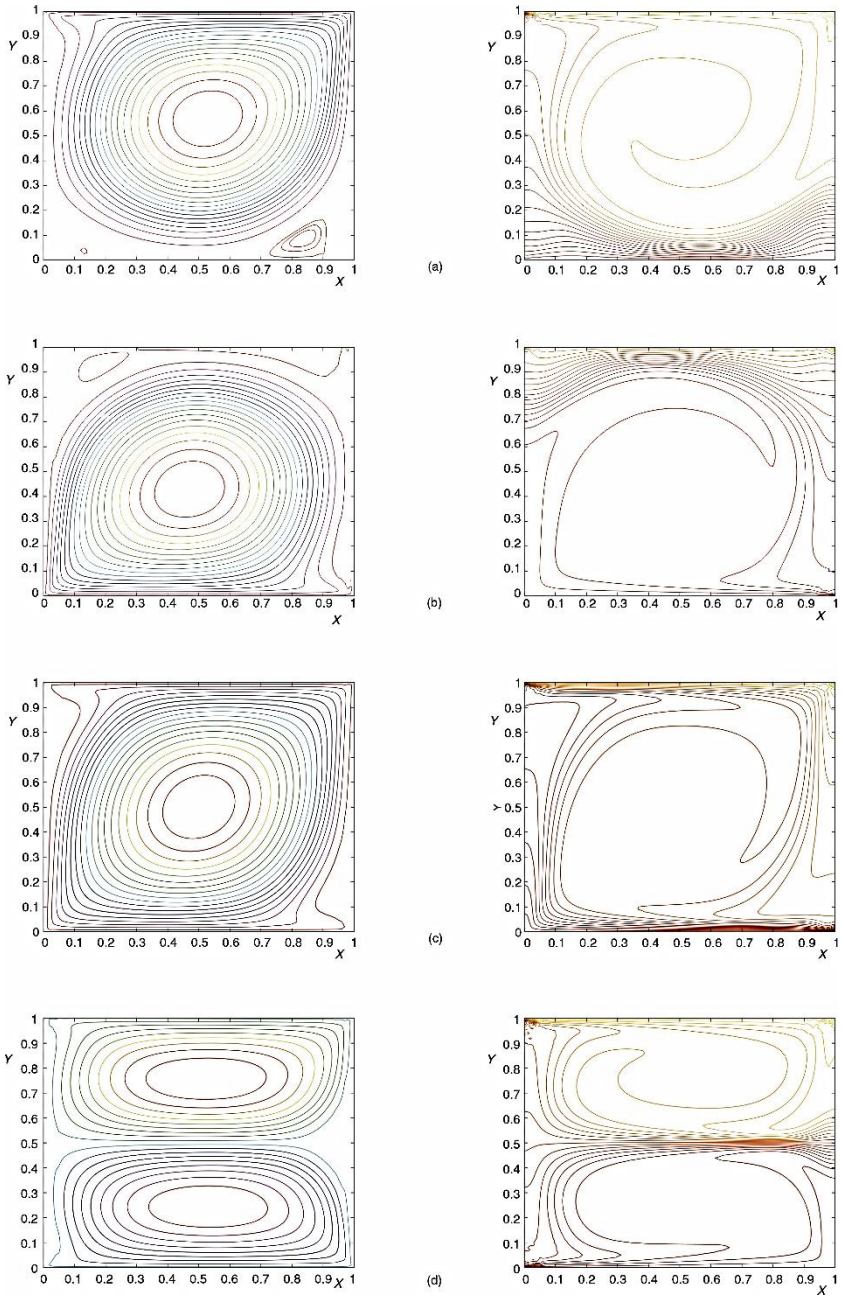

Figure 7. Temperatures and streamlines for four mixed convection simulations at $Re = 10^2$ and $Gr = 10^2$; (a) top lid-driven, (b) bottom lid-driven, (c) moving parallel, and (d) moving anti-parallel

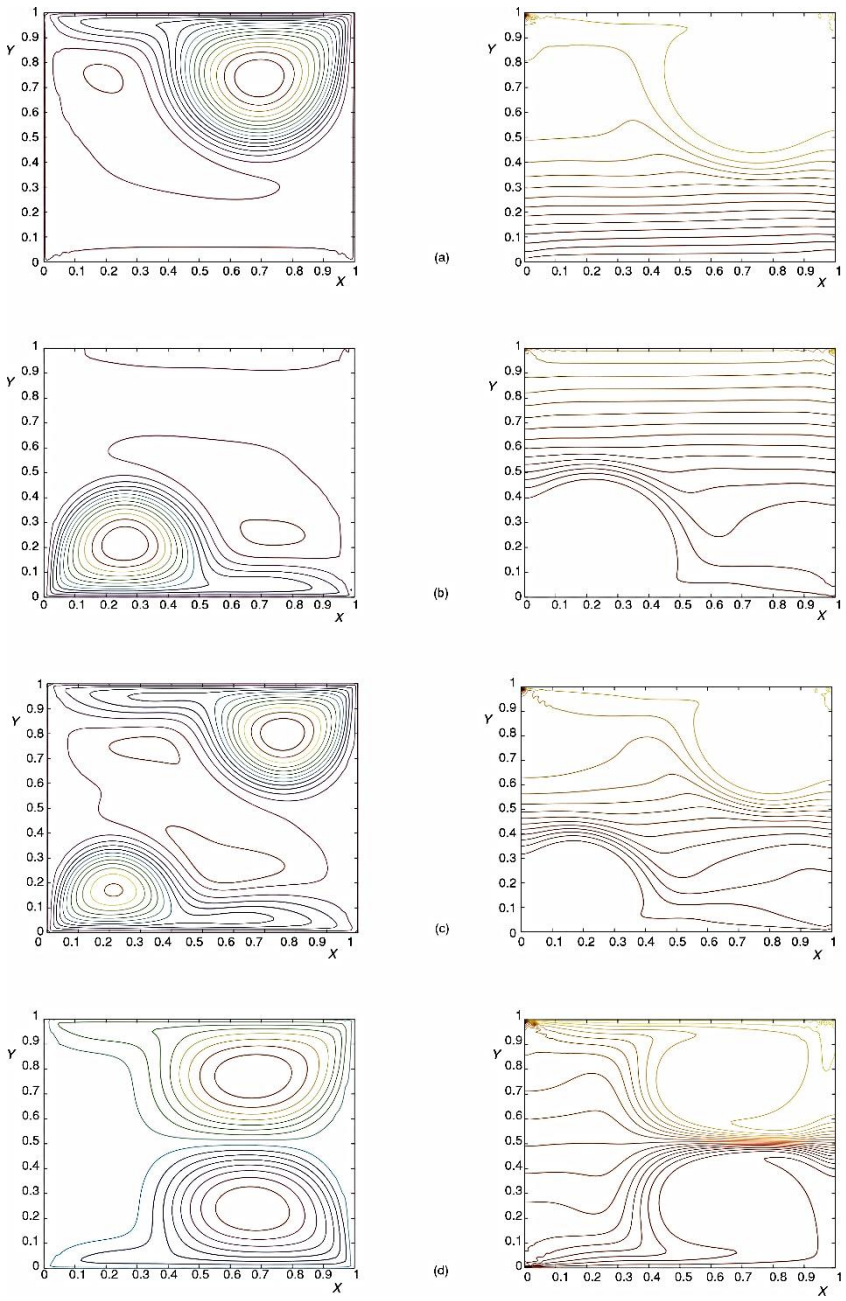

Figure 8. Temperatures and streamlines for four mixed convection simulations at $Re = 10^2$ and $Gr = 10^6$; (a) top lid-driven, (b) bottom lid-driven, (c) moving parallel, and (d) moving anti-parallel

The isotherms exhibit clustering near the lower lid, suggesting the presence of pronounced temperature gradients in the vertical direction within that area. However, in the majority of the cavity, except for this localized area, temperature gradients are not significant,

indicating the presence of strong mixing caused by mechanically induced circulations. As a result, there are minimal temperature differences in a significant portion of the interior region.

In contrast, in situations where buoyancy effects are dominant $\mathrm{Gr}/\mathrm{Re}^2 \ll 1$, as illustrated in figs. 8(a)-8(d), the fluid-flow and temperature fields display discernible characteristics. The interior circulation is currently limited to a confined area near the sliding top lid. The impact of the mechanically driven top lid is limited to a short distance within the interior region. The presence of stable stratification restricts vertical movements, leading to the accumulation of stagnant fluid within the central and lower interior regions. The vertical temperature stratification in these stagnant regions demonstrates a predominantly linear pattern, suggesting the occurrence of conductive heat transfer. It is worth mentioning that within a relatively confined area in the upper section of the cavity, fluids exhibit a relatively high degree of mixing, resulting in a relatively uniform temperature distribution. This particular region exhibits significant convective activities that are induced by mechanical forces.

In addition to the represented scenarios, we will now explore the implications of bottom-lid-driven motion with a velocity of U_0. When the upper and lower lids move with parallel velocities U_0, the flow patterns exhibit complexity, characterized by a primary circulation that extends throughout the entire cavity. The intricate fluid movements, as evidenced by the presence of minor cells in the corners, highlight the dynamic interaction between the walls in motion.

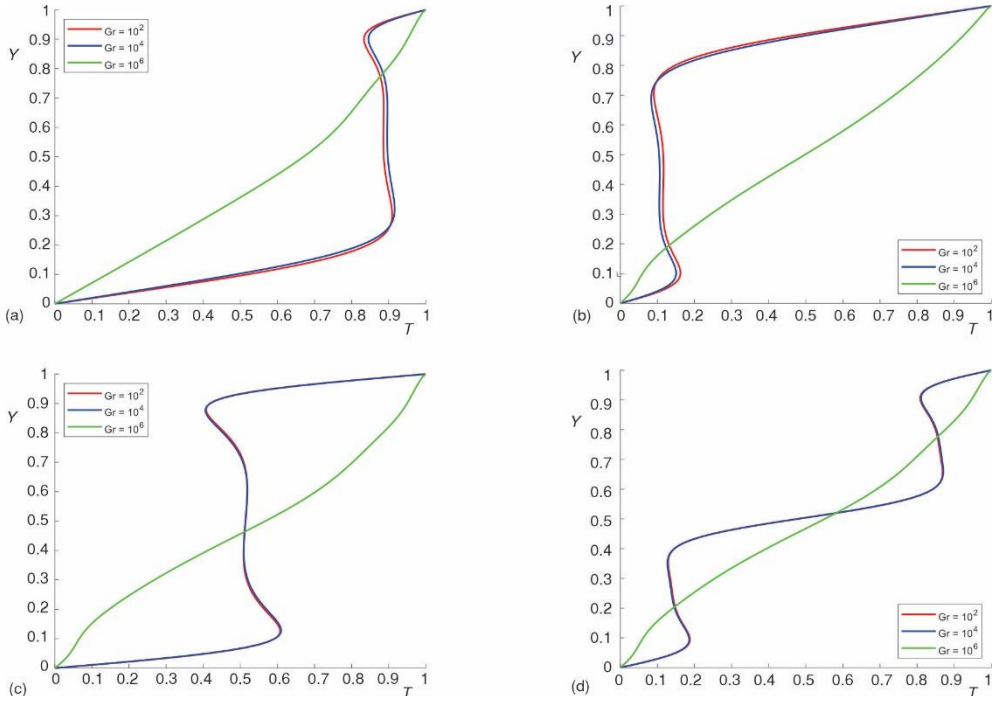

Figure 9. Temperature profile in the vertical direction along x = 0.5, Re = 400, and Pr = 0.71; (a) top lid-driven, (b) bottom lid-driven, (c) moving parallel, and (d) moving anti-parallel

Moreover, in the scenario where the upper lid exhibits a velocity of U_0 and the lower lid moves in the opposite direction with a velocity of $-U_0$, the resultant flow is predominantly

confined in proximity to the sliding upper lid. There are still substantial amounts of liquid in the bottom and middle sections, and most of the interior still has a constant vertical temperature differential. According to this, conduction is the primary means of heat transfer.

The data and analysis presented in its entirety offer a comprehensive representation of the interaction between buoyancy effects and different types of lid-driven movements, as well as their influence on fluid-flow and temperature distribution within the confined space. A detailed examination of different driving scenarios enhances our comprehension of the intricate dynamics of fluid motion in constrained systems.

The temperature profiles inside the cavity, limited by $T = 0$ at $y = 0$ and $T = 1$ at $y = 1$, differ significantly in four lid-driven cases in figs. 9(a)-9(d). Under the top lid-driven scenario, notable temperature variations appear near the upper lid when $\mathrm{Re} \to 0$ or when buoyancy effects are minimal ($\mathrm{Gr}/\mathrm{Re}^2 \ll 1$). Narrow strips next to the lids also undergo temperature changes. On the other hand, bottom lid-driven situations exhibit considerable temperature changes in the region of the lower lid when $\mathrm{Re} \to 0$ or when buoyancy effects are negligible. Variations are seen throughout the cavity with parallel motion, being more noticeable close to both lids as $\mathrm{Re} \to 0$. The $\mathrm{Re} \to 0$ or with minor buoyancy effects, which is anti-parallel motion and spreads temperature changes throughout the cavity, especially near the lids. These changes indicate how much the mechanical activity close to the lids affects the cavity's localized temperature distribution.

The total vertical heat transfer at a given height $y = y$ can be stated as:

$$\left[\frac{\partial T}{\partial y} - \mathrm{PrRe}\nu T\right] \tag{12}$$

The first and second components in this equation stand for the effects of convection and conduction, respectively, for top lid-driven. We can easily determine the relative relevance of these terms by examining the individual plots of these items in figs. 10(a)-10(d). The major role of conduction is indicated by $\mathrm{Gr} = 10^6$, where $\mathrm{Gr}/\mathrm{Re}^2 \gg 1$. In this case, throughout the majority of the cavity, $\partial T/\partial y \to 1$ and $-\mathrm{PrRe}\nu T \sim 0$. On the other hand, as indicated by the magnitudes of $-\mathrm{PrRe}\nu T$, convective heat transfer has a significant effect when $\mathrm{Gr}/\mathrm{Re}^2 < O(1)$, particularly in the middle and upper parts of the cavity. This in-depth analysis of the individual elements of eq. (12) confirms the previously mentioned qualitative tendencies.

It is important to examine how differences in boundary conditions, such as bottom lid-driven, moving parallel, or anti-parallel flows, would impact the relative dominance of conduction and convection in the system if we were to investigate similar scenarios. Even in a bottom lid-driven setting, these same patterns of conduction and convection dominance may exist. However, these particular localizations or magnitudes change based on the altered flow patterns and dynamics mixing.

Hence, it is critical to be able to determine flow direction and its effect on temperature gradients and the heat transfer process while also considering parallel or anti-parallel scenarios. The many organized variations may create possibilities for unique levels of convectional and conduction dominance that affect heat transport throughout the cavity.

Overall, this extensive comparison of the various flow situations demonstrates a highly useful process for determining how convection and conduction relate, showing what is more influential in specific situations.

When $\mathrm{Gr}/\mathrm{Re}^2$ is on the order of $O(1)$, figs. 11(a)-11(d) investigates the effect of the Prandtl number on global temperature fields, in situations where $\mathrm{Pr} \ll 1$, the temperature distribution is inclined to a vertically linear profile, indicating a high prevalence of conductive

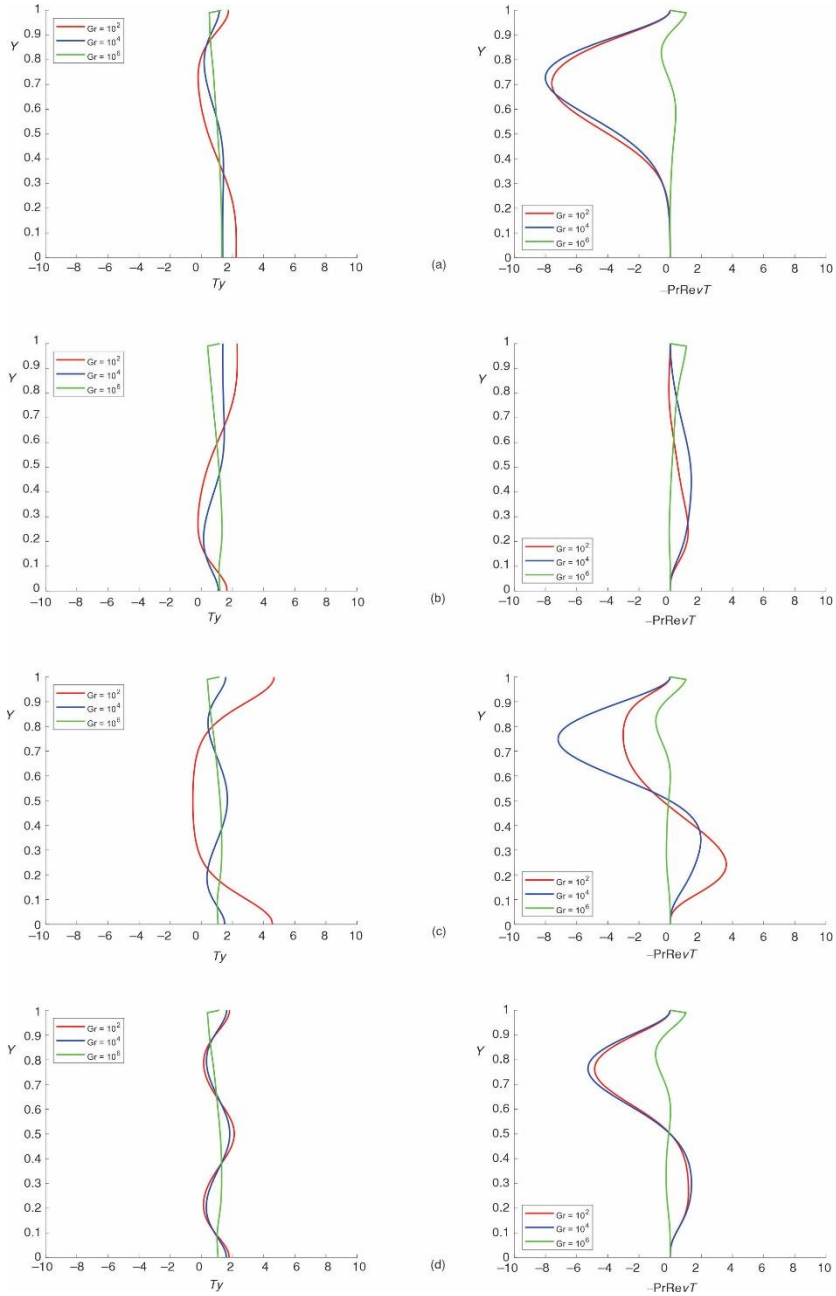

Figure 10. Verticle profiles of $\partial T/\partial y$ and $-\mathrm{PrRe}\nu T$ along $x = 0.5$, Re = 100, and Pr = 0.71; (a) top lid-driven, (b) bottom lid-driven, (c) moving parallel, and (d) moving anti-parallel

heat transfer. However, when Prandtl number is large, there is a very strong circulatory cell in the upper cavity. This creates a region of well-mixed fluids, and temperatures are reasonably uniform in the upper cavity. The bottom of the temperature field is a vertical linear, showing that the conductions mode dominates at the bottom.

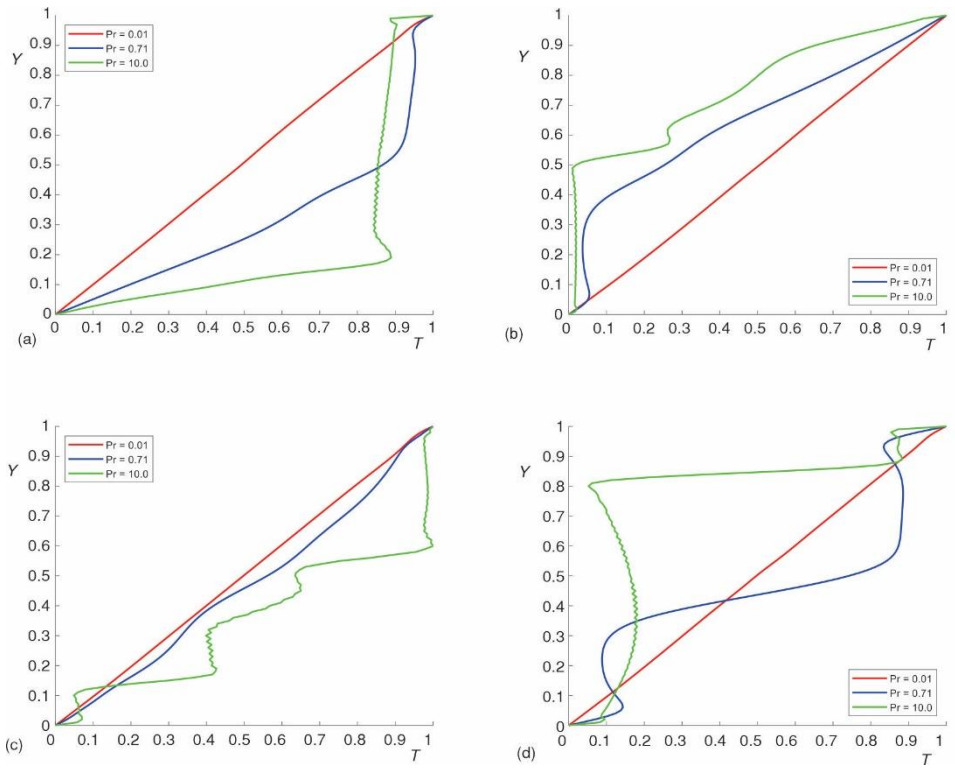

Figure 11. Temperature profile in the vertical direction along $x = 0.5$, Re = 10^3, and Gr 10^6; (a) top lid-driven, (b) bottom lid-driven, (c) moving parallel, and (d) moving anti-parallel

A feature in the temperature contours in the lower lid-driven scenarios is likely in a way similar to the findings in the upper lid-driven scenarios, particularly when it comes to temperature in the lower cavity area due to conduction. The vertical linear distribution of temperature at the bottom depicts the control of conductive heat transfer in that area of the cavity.

The temperature distribution in the cavity is strongly impacted by the direction and type of flow, particularly in parallel and antiparallel flow conditions. Unlike situations involving lid-driven movements, these changes can result in different temperature profiles and circulation patterns. For example, changing flow dynamics in parallel flows can lead to different temperature gradients and circulation cells, which can affect the magnitude of conduction and convection in various parts of the cavity.

Studying local changes in the Nusselt number along the top and bottom walls is essential when designing heat transfer equipment. For the top lid-driven scenario (Re = 400, Gr = 10^6, and Pr 0.71), as shown in figs. 12(a)-12(d), quiet fluid movements cause conduction-dominated heat transfer, which results in a Nusselt number at the bottom wall which is almost equal to unity. On the other hand, because of corner circulation, the sliding top wall displays a notable amount of convective heat transfer, which keeps the fluid temperatures close to the upper right corner consistent.

When bottom lid motion is taken into account, the bottom wall exhibits low convective heat transfer, similar to near-unity Nusselt number, whereas the top wall shows

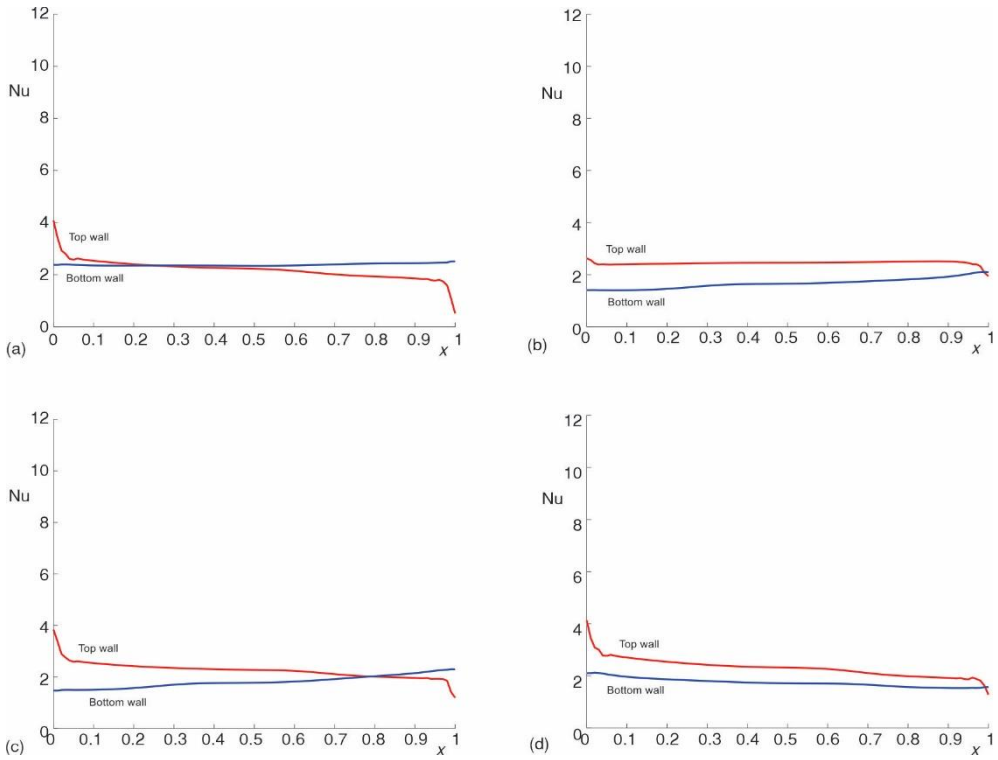

Figure 12. Local Nusselt number profiles at the top and bottom walls. Profiles are along the top wall, $y = 1$ and the bottom wall, $y = 0$, Re = 400, Gr = 10^6, and Pr 0.71; (a) top lid-driven, (b) bottom lid-driven, (c) moving parallel, and (d) moving anti-parallel

higher convective heat transfer in the region of the upper left corner. Both walls show comparable Nusselt number in situations of parallel motion, with conduction predominating and convective effects being less noticeable near the corners. On the other hand, because anti-parallel motion results in low convective heat transfer for both walls, Nusselt number remains appropriately near unity despite opposing motions, and the fluid temperature distribution in the system is generally uniform.

Local Nusselt number changes (Re = 400, Gr = 10^2, and Pr = 0.71) under convective activity situations are shown in figs. 13(a)-13(d). Nusselt number profiles at the two boundary walls show considerable fluid-flow, which significantly improves heat transfer in the cavity. This fundamental understanding will be essential for those designing useful heat exchangers. Furthermore, these numerical results provide crucial baselines against which future numerical or observational data can be compared. Analysis of motion generated by the bottom lid reveals enhanced convective activity at both sides, hence enhancing heat transfer in the system. Increased fluid movements at the borders also improve heat transmission in parallel motion, where both walls move in the same direction. In contrast, anti-parallel motion demonstrates enhanced convective activity along the opposite walls, providing more insight into how directed motions affect heat transfer inside the cavity.

We may evaluate the given Nusselt number values at various Grashof number to identify the most efficient scenario among the four (top lid-driven, bottom lid-driven, both walls moving parallel, and both walls moving anti-parallel) at Re = 400. Higher values of the Nusselt number a dimensionless measure indicating convective heat transfer, represent superior heat transfer.

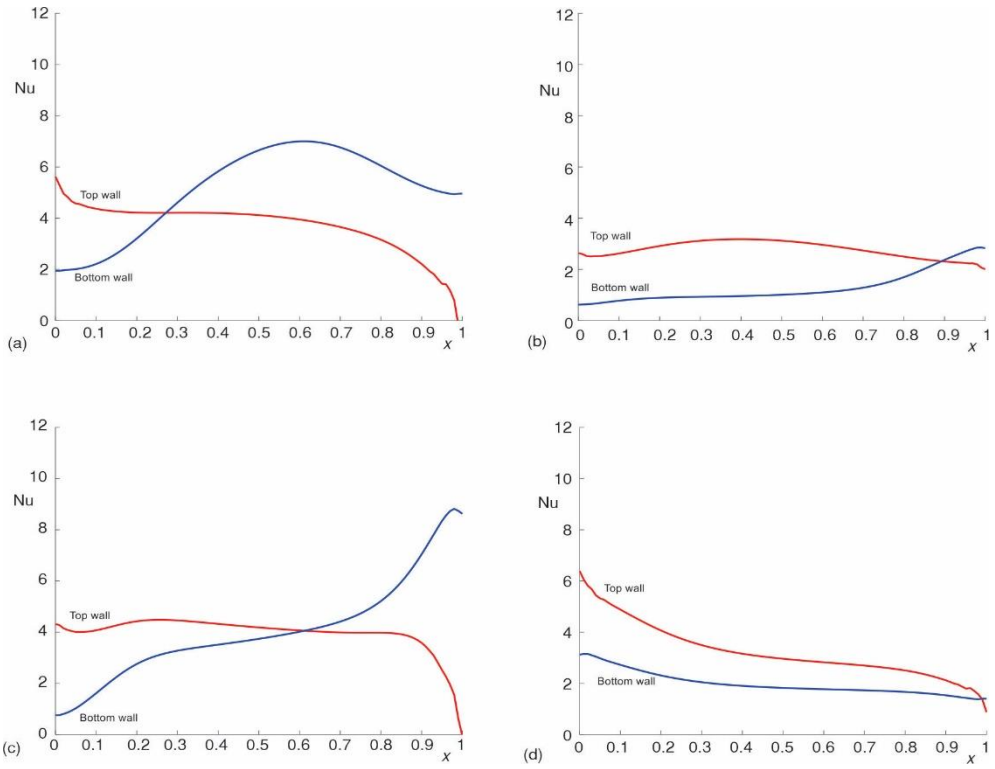

Figure 13. Local Nusselt number profiles at the top and bottom walls. Profiles are along the top wall, $y = 1$ and the bottom wall, $y = 0$, Re = 400, Gr = 10^2, and Pr = 0.71; (a) top lid-driven, (b) bottom lid-driven, (c) moving parallel, and (d) moving anti-parallel

Tables 4 and 5 below compare the Nusselt number values at Re = 400 and various Grashof number and also compare the results of Nusselt number at the top wall.

Table 5. The Nusselt number at the top wall in Re = 400 and Gr = 10^2, 10^4, 10^6

Grashof number	Top lid-driven	Bottom lid-driven	Moving parallel	Moving Anti-parallel
10^2	3.74	3.18	4.48	4.26
10^4	3.71	3.11	4.47	4.26
10^6	1.29	1.15	2.40	2.38

Table 4. Comparing the average Nusselt number in Re = 400 and Gr = 10^2, 10^4, 10^6

Grashof number	Present results	Iwatsu *et al*. [10]	Difference [%]
10^2	3.74	3.84	2.60
10^4	3.71	3.62	2.49
10^6	1.29	1.22	5.42

In examining the data, it seems that the scenario with *Both walls moving parallel* always produces the highest Nusselt number for all Grashof number. Therefore, this arrangement works better for convective heat transmission at Re = 400. This superiority could be explained by certain flow patterns, vortices, or other fluid dynamics related to *Both walls moving parallel* scenarios, which would improve heat transfer.

Conclusions

Examining mixed convective flow and heat transfer in a driven-cavity with an aspect ratio of $O(1)$ and an enforced temperature difference at the system borders of $\Delta T\left(\equiv T_{\mathrm{h}} - T_0\right) > 0$ displays interesting behavior. After initially concentrating on the top lid-driven case, several behaviors were observed concerning $\mathrm{Gr/Re}^2$ ratios. Forced convection is dominant when $\mathrm{Gr/Re}^2 \ll 1$, producing well-mixed fluids in the middle areas and concentrated isotherms next to the walls. On the other hand, buoyancy-driven convective characteristics take center stage when $\mathrm{Gr/Re}^2 \gg 1$, resulting in stagnant lower and intermediate areas with vertically linear temperature distributions and near-horizontal isotherms.

The knowledge was expanded by extending the research to include bottom lid-driven, parallel motion, and anti-parallel motion instances. These differences clarified subtle effects, particularly in the driving force's penetration depth, the development of stationary regions, and temperature distribution profiles. Furthermore, the impact of Prandtl number at $\mathrm{Gr/Re}^2 \sim O(1)$ revealed significant differences: lower Prandtl number values produced temperature profiles that were vertically linear in the cavity's inside, whereas higher Prandtl number values promoted well-mixed upper cavity regions but showed vertically linear distributions in the lower part.

It is interesting concerning these results that the situation with both walls moving parallel showed consistently better convective heat transfer characteristics at different ratios of $\mathrm{Gr/Re}^2$. This suggests that the cavity's heat transmission efficiency is improved by the walls moving in parallel. The complex interactions between driving processes applied temperature differences, and distinct cavity shapes on mixed convective flow and heat transfer are highlighted in this extensive research. The enforced $\Delta T\left(\equiv T_{\mathrm{h}} - T_0\right) > 0$ condition highlights the significance of temperature differences on fluid behavior in restricted cavities, hence emphasizing these small details.

Nomenclature

A – aspect ratio, [~O(1)], [–]
b – width of the cavity, [m]
h – height of the cavity, [m]
$\boldsymbol{e}$ – unit vector in the direction of buoyancy forces, [–]
$\boldsymbol{e}_i$ – discrete particle velocity, [–]
F^{eq} – equilibrium distribution function for fluid-flow, [–]
f – buoyancy force term, [–]
G^{eq} – equilibrium distribution function for the temperature of the fluid field, [–]
Gr – Grashof number [=g$\beta W^3(T_{\mathrm{h}} - T_{\mathrm{c}})/\nu^2$], [–]
Nu – Nusselt number (=hL/k), [–]
Pr – Prandtl number (=ν/α), [–]
$\hat{p}$ – pressure, [Pa]
Ra – Rayleigh number (=Gr×Pr), [–]
Re – Reynold number (=$U_0 b/\nu$), [–]
Ri – Richardson number (=$\mathrm{Gr/Re}^2$), [–]
$\boldsymbol{r}$ – position of a particle, [–]
T – dimensionless temperature, [–]
T_{h} – temperature of the top wall, [–]
T_0 – temperature of the bottom wall, [–]
t – time, [s]
U_0 – dimensionless lid velocity, [–]
u,v – horizontal and vertical components of velocity, [ms^{-1}]
x,y – horizontal and vertical co-ordinate, [m]

Greek symbol

α – thermal diffusivity, [m^{2}s^{-1}]
ν – fluid kinematic viscosity, [m^{2}s^{-1}]
ρ – fluid density, [kgm^{-3}]
τ_v – relaxation time for flow, [s]
τ_T – relaxation time for temperature, [s]
ω_i – weighting factors, [–]

References

[1] Khemici, M., *et al.*, Numerical Study of Developing Laminar Mixed Convection in a Heated Annular Duct with Temperature Dependent Properties, *Thermal Science*, *23* (2019), 6A, pp. 3411-3423

[2] Guo, Z., *et al.,* Discrete Lattice Effects on the Forcing Term in the Lattice Boltzmann Method, *Physical review E*, *65* (2002), 4, 046308
[3] Mohamad, A. A., Kuzmin, A., A Critical Evaluation of Force Term in Lattice Boltzmann Method, Natural Convection Problem, *International Journal of Heat and Mass Transfer*, *53* (2010), 5-6, pp. 990-996
[4] Koseff, J. R., Street, R. L., The Lid-Driven Cavity Flow: A Synthesis of Qualitative and Quantitative Observations, *Journal of Fluids Engineering*, *106* (1984), 4, pp. 390-398
[5] Ghia, U., *et al.*, High-Re Solutions for Incompressible Flow Using the Navier-Stokes Equations and a Multigrid Method, *Journal of Computational Physics*, *48* (1982), 3, pp. 387-411
[6] Schreiber, R., Keller, H. B., Driven Cavity Flows by Efficient Numerical Techniques, *Journal of Computational Physics*, *49* (1983), 2, pp. 310-333
[7] Laidoudi, H., Bouzit, M., Mixed Convection in Poiseuille Fluid From an Asymmetrically Confined Heated Circular Cylinder, *Thermal Science*, *22* (2018), 2, pp. 821-834
[8] Jan, A., *et al.*, Heat Transfer Enhancement of Forced Convection Magnetized Cross Model Ternary Hybrid Nanofluid-flow Over a Stretching Cylinder: Non-Similar Analysis, *International Journal of Heat and Fluid-flow*, *106* (2024), 109302
[9] Ullah, A., *et al.*, Control of Irregular Flows and Fluid Forces Around Two Offset Cylinders in the Presence of Control Plate, *J. of the Brazilian Society of Mechanical Sciences and Engineering*, *46* (2024), 8, 460
[10] Iwatsu, R., *et al.*, Mixed Convection in a Driven Cavity with a Stable Vertical Temperature Gradient, *International Journal of Heat and Mass Transfer*, *36* (1993), 6, pp. 1601-1608
[11] Mohamad, A. A., Viskanta, R., Combined Surface Shear and Buoyancy-Driven Convection in a Shallow Cavity, *Fundamentals of Natural Convection*, *140* (1990), pp. 1-7
[12] Karimipour, A., *et al.*, Mixed Convection of Copper–Water Nanofluid in a Shallow Inclined Lid Driven Cavity Using the Lattice Boltzmann Method, *Physica A: Statistical Mechanics and its Applications*, *402* (2014), May, pp. 150-168
[13] Guo, Y., *et al.*, Simulation of Mixed Convection in Slender Rectangular Cavity with Lattice Boltzmann Method, *International Journal of Numerical Methods for Heat & Fluid-flow*, *20* (2010), 1, pp. 130-148
[14] Bettaibi, S., *et al.*, Lattice Boltzmann Simulation of Mixed Convection Heat Transfer in a Driven Cavity with Non-Uniform Heating of the Bottom Wall, *Communications in Theoretical Physics*, *63* (2015), 1, pp. 91-100
[15] Abu-Nada, E., Chamkha, A. J., Mixed Convection Flow of a Nanofluid in a Lid-Driven Cavity with a Wavy Wall, *International Communications in Heat and Mass Transfer*, *57* (2014), Oct., pp. 36-47
[16] Oztop, H. F., *et al.*, MHD Mixed Convection in a Lid-Driven Cavity with Corner Heater, *International Journal of Heat and Mass Transfer*, *54* (2011), 15-16, pp. 3494-3504
[17] Peng, Y., *et al.*, Simplified Thermal Lattice Boltzmann Model for Incompressible Thermal Flows, *Physical Review E*, *68* (2003), 2, 026701
[18] Chen, H., Teixeira, C., H-Theorem and Origins of Instability in Thermal Lattice Boltzmann Models, *Computer Physics Communications*, *129* (2000), 1-3, pp. 21-31
[19] Zou, Q., He, X., On Pressure and Velocity Boundary Conditions for the Lattice Boltzmann BGK Model, *Physics of Fluids*, *9* (1997), 6, pp. 1591-1598
[20] Bhatnagar, P. L., *et al.*, A Model for Collision Processes in Gases. I. Small Amplitude Processes in Charged and Neutral One-Component Systems, *Physical Review*, *94* (1954), 3, pp. 511-525
[21] Hafeez, M. A., Islam, S. U., Mixed Convection in a Driven Cavity with an Internal Obstacle Using the Lattice Boltzmann Method, *Thermal Science*, *26* (2022), 6B, pp. 5211-5226

Paper submitted: June 27, 2024
Paper revised: August 2, 2024
Paper accepted: August 14, 2024